Letter

Spontaneous square versus hexagonal nanoscale skyrmion lattices in Fe/Ir(111)

Mara Gutzeit,[1] Tim Drevelow,[1] Moritz A. Goerzen,[1] Soumyajyoti Haldar,[1,*] and Stefan Heinze[1,2]
[1]*Institute of Theoretical Physics and Astrophysics, University of Kiel, Leibnizstrasse 15, 24098 Kiel, Germany*
[2]*Kiel Nano, Surface, and Interface Science (KiNSIS), University of Kiel, Kiel, Germany*

(Received 31 January 2023; revised 19 June 2023; accepted 10 August 2023; published 24 August 2023)

We study the emergence of spontaneous skyrmion lattices in an Fe monolayer in fcc and hcp stacking on the Ir(111) surface using density functional theory (DFT). For fcc-Fe/Ir(111) we find the well-known square nanoskyrmion lattice. However, for hcp-Fe/Ir(111) the hexagonal skyrmion lattice previously proposed based on experiments is energetically unfavorable with respect to a hexagonal multi-Q state with nearly collinear magnetic moments. By mapping our DFT calculations to an atomistic spin model we demonstrate that the interplay of pairwise exchange, higher-order exchange, and Dzyaloshinskii-Moriya interaction is decisive for the symmetry and collinearity of the obtained spin lattice.

DOI: 10.1103/PhysRevB.108.L060405

Spintronics using noncollinear spin textures has been a rapidly growing field since the experimental discovery of magnetic skyrmion lattices [1–3]. Skyrmions have been observed in a large variety of magnetic materials even at room temperature [4–6] and numerous potential applications of magnetic skyrmions [7] are currently being explored [8,9]. The origin of skyrmions is the Dzyaloshinskii-Moriya interaction (DMI) [10,11] which occurs due to spin-orbit coupling in systems with broken inversion symmetry and favors canted spin structures with a unique rotational sense [12]. It has been shown that frustrated or higher-order exchange can stabilize nanoscale topological spin structures as well [13–16]. Higher-order exchange interactions such as the four-spin interaction can also lead to multi-Q states which are a superposition of single-Q (spin spiral) states [17–23].

The formation of a spontaneous nanoskyrmion lattice in an Fe monolayer (ML) grown in fcc stacking on the Ir(111) surface, denoted as fcc-Fe/Ir(111), is caused by the interplay of DMI and the four-spin exchange interaction [3]. Recently, it has been demonstrated that there are actually two types of four-spin exchange terms [24]. This can explain the collinear up-up-down-down ($uudd$) ground state—a $2Q$ state formed from the superposition of two 90° spin spirals—of an Fe ML on Rh(111) [18] and the slightly canted $uudd$ state found in Rh/Fe/Ir(111) [19]. The newly proposed three-site four-spin interaction [24] can also lead to two-dimensional nearly collinear multi-Q states as observed in an Fe ML in hcp stacking on Rh/Ir(111) [25]. In contrast to the square nanoskyrmion lattice of fcc-Fe/Ir(111) [3] these collinear multi-Q states possess a hexagonal unit cell. For hcp-Fe/Ir(111) a hexagonal magnetic state has been observed using spin-polarized scanning tunneling microscopy (SP-STM) and interpreted based on the experimental data as a nanoskyrmion lattice [26]. However, a first-principles study of hcp-Fe/Ir(111) has been missing so far.

Here, we investigate the Fe monolayer in both fcc and hcp stacking on Ir(111) by means of first-principles calculations based on density functional theory (DFT). We find that a noncollinear square nanoskyrmion lattice is the magnetic ground state of fcc-Fe/Ir(111) in accordance with previous work [3]. Surprisingly, a nearly collinear hexagonal multi-Q state is revealed to be lowest in energy for hcp-Fe/Ir(111) in contrast to the hexagonal noncollinear skyrmion lattice previously proposed based on spin-polarized scanning tunneling microscopy measurements [26]. In order to understand the stabilization mechanisms of spontaneous skyrmion lattices with different symmetries and degrees of noncollinearity we map total DFT energies of a variety of complex magnetic structures to an atomistic spin model. We reveal that in Fe/Ir(111) the interplay of pairwise Heisenberg exchange, Dzyaloshinskii-Moriya interaction (DMI), and higher-order exchange interactions favors a high degree of noncollinearity in square nanoskyrmion lattices while it leads to nearly collinear spin alignments in hexagonal spin lattices.

We start by discussing the energy dispersion $E(\mathbf{q})$ of flat spin spirals for both stackings of the Fe ML on Ir(111) (Fig. 1 and Supplemental Fig. S1 [27]) obtained via DFT calculations using the FLEUR code [28] (see Supplemental Material [27] for computational details). Spin spirals are characterized by a $\mathbf{q}$ vector from the irreducible part of the two-dimensional hexagonal Brillouin zone (2D BZ). They represent the general solution of the Heisenberg model on a periodic lattice and thus allow to scan a large part of the magnetic phase space. For a spin spiral with a specific wave vector $\mathbf{q}$ the direction of a magnetic moment at lattice site $\mathbf{R}_i$ is given by $\mathbf{M}_i = M(\cos(\mathbf{q}\cdot\mathbf{R}_i), \sin(\mathbf{q}\cdot\mathbf{R}_i), 0)$, with M denoting the size of the magnetic moment. The calculated Fe magnetic moments are $M_{\mathrm{Fe}} \approx 2.72\mu_B$ for fcc-Fe/Ir(111) and $\approx 2.71\mu_B$ for hcp-Fe/Ir(111), respectively, and are quite stable upon the variation of $\mathbf{q}$.

We find a large exchange frustration for both Fe stackings. For hcp-Fe/Ir(111) (Fig. 1), the energy dispersion neglecting spin-orbit coupling is quite flat around the ferromagnetic (FM)

*Corresponding author: haldar@physik.uni-kiel.de

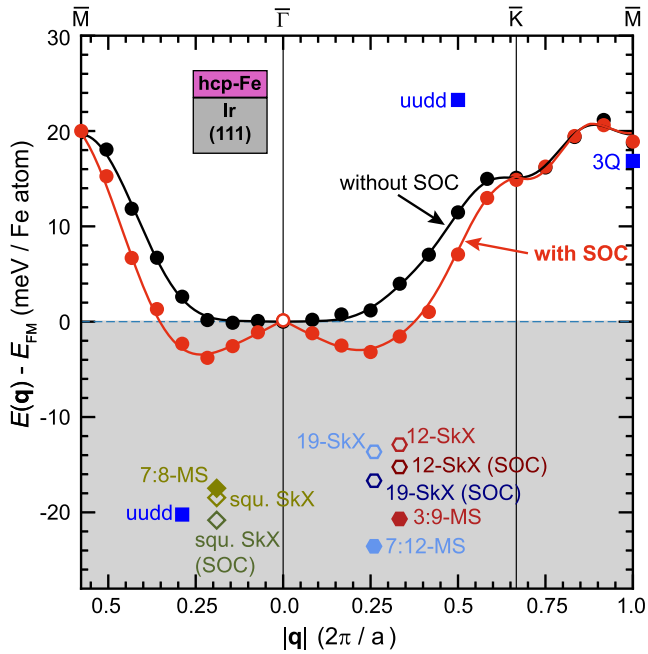

FIG. 1. Energy dispersion $E(\mathbf{q})$ of flat cycloidal spin spirals calculated via DFT along the two high-symmetry directions of the two-dimensional Brillouin zone for hcp-Fe/Ir(111). Black (red) circles represent total DFT energies without (with) spin-orbit coupling (SOC), while black (red) lines show a fit to the Heisenberg model neglecting (including) DMI. The DFT total energies of several multi-Q states discussed in the text are denoted at the $\mathbf{q}$ values of their constituting single-Q states.

state at the $\overline{\Gamma}$ point. The row-wise antiferromagnetic (RW-AFM) state at the $\overline{M}$ point is by about 20 meV/Fe atom higher in energy than the FM state. For fcc-Fe/Ir(111) (Fig. S1 [27]), a similar picture emerges, however, the FM state represents a local energy maximum while spin spirals with periods of $\lambda = 1.9$–1.7 nm ($q = |\mathbf{q}| \approx 0.14$–$0.16 \times 2\pi/a$) along both high-symmetry directions experience a small energy gain of 2–4 meV/Fe atom. Mapping the DFT results to the Heisenberg model of pairwise exchange (black lines) reveals a small FM nearest-neighbor exchange constant which competes with AFM interactions of second- and third-nearest neighbors (see Table I).

The inclusion of spin-orbit coupling (SOC) in DFT calculations (Fig. 1) generates energy minima in hcp-Fe/Ir(111) for cycloidal spin spirals with periods of $\lambda = 1.4$–1.1 nm ($q = |\mathbf{q}| \approx 0.20$–$0.25 \times 2\pi/a$) with a depth of up to 4 meV/Fe

TABLE I. Heisenberg exchange constants for the first three nearest neighbors, J_1–J_3, as extracted from the fit of the respective energy dispersion (without modification by higher-order interaction terms) and the higher-order exchange constants B_1, K_1, and Y_1 calculated using the pseudoinverse method (see Supplemental Material [27] for details). All values are given in meV.

System	J_1	J_2	J_3	B_1	K_1	Y_1
fcc-Fe/Ir(111)	5.46	−1.35	−1.24	−1.97	−2.22	2.47
hcp-Fe/Ir(111)	2.52	−0.24	−1.03	0.42	−2.09	0.68

atom and further stabilizes the spin spiral minima in fcc-Fe/Ir(111). The energy contributions due to SOC for every spin spiral state (Fig. S2 [27]) reveal the preference of a clockwise rotational sense of cycloidal spin spirals for both Fe stackings with a nearest-neighbor DMI constant of about 1.6 meV (see Supplemental Material [27] for all DMI constants).

To go beyond spin spiral (single-Q) states and search for the experimentally observed square and hexagonal spin lattices [3,26], we have calculated the total DFT energies of several multi-Q states. We find that for both Fe stackings the collinear *uudd* ($2Q$) state along the $\overline{\Gamma M}$ direction is much lower in energy than all spin spiral states (Fig. 1 and Fig. S1). In contrast, the *uudd*-$\overline{\Gamma K}$ state and the triple-Q state are on the order of 20–40 meV/Fe atom above the FM state. Within the Heisenberg model of pairwise exchange a multi-Q state and its corresponding spin spiral ($1Q$) state are energetically degenerate. Therefore, the large energy differences obtained in our DFT calculations indicate significant higher-order exchange contributions.

We have further considered the square nanoskyrmion lattice (squ SkX) observed in fcc-Fe/Ir(111) [3] that is constructed from a superposition of two $\mathbf{q}$ vectors enclosing an angle of about 90° [Fig. 2(a)]. In the scalar-relativistic calculation this state is energetically slightly above the *uudd* state (Fig. 1). However, the inclusion of SOC significantly lowers its energy by about 2 meV/Fe atom for both stackings. By projecting the magnetic moments of the squ SkX onto the z axis perpendicular to the film plane we obtain a fully collinear state with seven moments pointing in one and eight pointing into the opposite direction, the 7:8-mosaic state (MS) [Fig. 2(b)] [29]. In both systems, this state is energetically clearly unfavorable compared to the squ SkX (Fig. 1 and Fig. S1).

Hexagonal skyrmion lattices can be constructed from the superposition of three $\mathbf{q}$ vectors of equal lengths and with angles of 120° between them [25]. If one chooses the $\mathbf{q}$ vectors along the symmetry-equivalent $\overline{\Gamma K}$ directions and with a period of three nearest-neighbor distances one obtains a hexagonal 12 atom SkX [Fig. 2(c)] previously proposed as the magnetic ground state of hcp-Fe/Ir(111) [26]. The total DFT energy of the hex 12-SkX is lower than the spin spiral minimum [30] but significantly above the squ SkX (Fig. 1). Surprisingly, the collinear analog, the 3:9-MS [Fig. 2(d)], gains energy with respect to the corresponding hex 12-SkX for both Fe stackings. This effect is even more prominent in hcp-Fe/Ir(111) (Fig. 1) and brings the energy of the 3:9-MS below the *uudd*-$\overline{\Gamma M}$ state and to the same energy as the square SkX.

A similar scenario emerges for the hexagonal 19-SkX versus the collinear 7:12-MS which are constructed in an analogous way with shorter and slightly rotated $\mathbf{q}$ vectors [Figs. 2(e) and 2(f)]. The collinear 7:12-MS, which has previously been observed in hcp-Fe/Rh/Rh/Ir(111) [25], is energetically lower than the noncollinear hexagonal 19-SkX (Fig. 1). For hcp-Fe/Ir(111) the 7:12-MS state is energetically even lower than the 3:9-MS and the square SkX (Fig. 1).

Note that experimentally a hexagonal magnetic structure with 12 atoms per unit cell, consistent with the 3:9-MS or the 12-SkX, has been observed in hcp-Fe/Ir(111) using

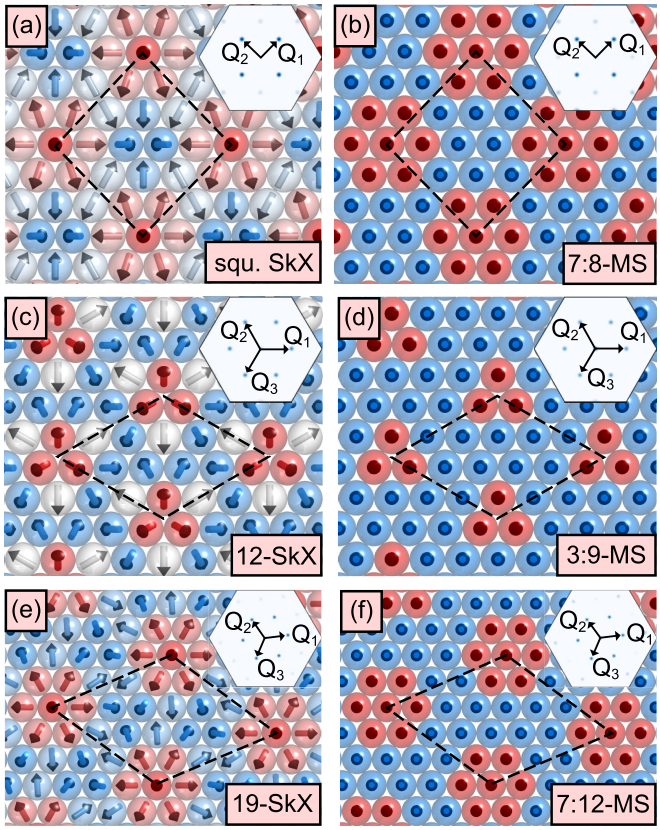

FIG. 2. Sketches of selected multi-Q states in Fe/Ir(111) with their respective unit cells indicated by dashed lines. (a) The square nanoskyrmion lattice observed in fcc-Fe/Ir(111) [3] and (b) the corresponding collinear 7:8-MS. (c) The hexagonal 12-atomic skyrmion lattice proposed as the magnetic ground state of hcp-Fe/Ir(111) [26] and (d) the corresponding collinear 3:9-MS. (e) The hexagonal 19-atomic skyrmion lattice and (f) the corresponding collinear 7:12-MS. Spheres illustrate Fe atoms and arrows the direction of their magnetic moments in which red (blue) denotes the up (down) out-of-plane component. Insets show the Fourier transform of the spin structures in the hexagonal Brillouin zone and the two (three) **Q** vectors from which the square (hexagonal) skyrmion lattices are constructed.

SP-STM [26], while in our DFT calculation the 7:12-MS is slightly lower in total energy (Fig. 1). Nevertheless, the trend favoring a *hexagonal collinear* rather than a *square noncollinear* spin lattice for hcp-Fe stacking can clearly be recognized from our DFT calculation. In contrast, the noncollinear square SkX is the energetically lowest state for fcc-Fe/Ir(111) in accordance with previous work (Fig. S1 [27]) [3].

In order to explain the microscopic origin of a collinear hexagonal mosaic state in hcp-Fe/Ir(111) versus a noncollinear square nanoskyrmion lattice in fcc-Fe/Ir(111) we consider an atomistic spin model given by

$$\begin{aligned} H = &-\sum_{ij} J_{ij}(\mathbf{m}_i \cdot \mathbf{m}_j) - \sum_{ij} \mathbf{D}_{ij}(\mathbf{m}_i \times \mathbf{m}_j) \\ &- \sum_{i} K_u \left(m_i^z\right)^2 - \sum_{\langle ij \rangle} B_1(\mathbf{m}_i \cdot \mathbf{m}_j)^2 \\ &- \sum_{\langle ijkl \rangle} K_1[(\mathbf{m}_i \cdot \mathbf{m}_j)(\mathbf{m}_k \cdot \mathbf{m}_l) + (\mathbf{m}_i \cdot \mathbf{m}_l)(\mathbf{m}_j \cdot \mathbf{m}_k) \\ &-(\mathbf{m}_i \cdot \mathbf{m}_k)(\mathbf{m}_j \cdot \mathbf{m}_l)] \\ &- \sum_{\langle ijk \rangle} Y_1[(\mathbf{m}_i \cdot \mathbf{m}_j)(\mathbf{m}_j \cdot \mathbf{m}_k) + (\mathbf{m}_j \cdot \mathbf{m}_i)(\mathbf{m}_i \cdot \mathbf{m}_k) \\ &+(\mathbf{m}_i \cdot \mathbf{m}_k)(\mathbf{m}_k \cdot \mathbf{m}_j)]. \end{aligned} \tag{1}$$

Here, $\mathbf{m}_i = \mathbf{M}_i/M$ denotes the normalized magnetic moment at lattice site i, J_{ij} the Heisenberg pairwise exchange constants, $\mathbf{D}_{ij}$ the vectors of the DMI, and K_u the uniaxial magnetocrystalline anisotropy constant. The last three terms are the higher-order exchange interactions arising from fourth-order perturbation theory from a multiband Hubbard model [24]. We restrict ourselves to the nearest-neighbor approximation as suggested in Ref. [24] and the coupling strengths are B_1, K_1, and Y_1 for the biquadratic, four-site four-spin, and three-site four-spin interactions, respectively (Table I). All interaction constants of the atomistic spin model, given by Eq. (1), were determined from DFT total energies (see Supplemental Material [27] for details).

Figure 3 shows the energy of the energetically lowest states of Fe/Ir(111) computed from the atomistic spin model [31]. The trend of DFT energies for the multi-Q states is captured by the atomistic spin model (top panels of Fig. 3). In particular, the collinear 3:9-MS and 7:12-MS are energetically preferred over the hexagonal 12-SkX and 19-SkX, respectively. In contrast, the noncollinear square SkX is lower in energy than the collinear 7:8-MS, in agreement with DFT. The model also correctly predicts the square SkX as the magnetic ground state of fcc-Fe/Ir(111) and in the case of hcp-Fe/Ir(111) the hexagonal 3:9-MS is the state of lowest energy [32].

By decomposing the total energy from the spin model into the single interaction contributions one can study how the differences between square and hexagonal skyrmion lattices arise (lower panels in Fig. 3). The four-site four-spin interaction ($K_1 < 0$) leads to a coupling of $1Q$ (spin spiral) states to multi-Q states as previously reported for fcc-Fe/Ir(111) [3]. For example, the *uudd*-$\overline{\Gamma M}$ state is preferred by about 20 meV/Fe atom with respect to the 90°-$1Q$-$\overline{\Gamma M}$ spin spiral state (Fig. 3) and a similar energy gain is obtained for skyrmion lattices and mosaic states versus $1Q$ states. Note that the three mosaic states gain the largest amount of energy by the four-site four-spin interaction.

The three-site four-spin interaction with its positive sign ($Y_1 > 0$) promotes collinear over noncollinear spin states with a considerable preference for hexagonal spin lattices. This effect has previously been reported to stabilize collinear hexagonal multi-Q states in Fe/Rh/Ir(111) [25]. A decisive role is played by the biquadratic term. Due to its sign, it favors noncollinear states over collinear states for fcc-Fe stacking ($B_1 < 0$) and vice versa for hcp-Fe stacking ($B_1 > 0$). Thereby, the square SkX becomes the energetically lowest state for fcc-Fe/Ir(111), while the hexagonal 3:9-MS is favored for hcp-Fe/Ir(111).

To obtain deeper insight into the question why the square spin lattice is noncollinear while the hexagonal spin lattices are collinear, we have calculated via DFT the total energies

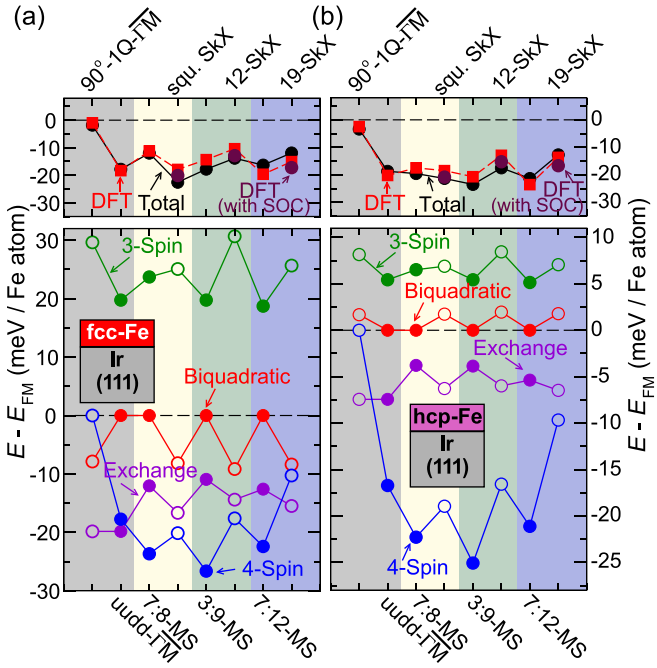

FIG. 3. Spin model vs DFT total energies for selected magnetic states in (a) fcc-Fe/Ir(111) and (b) hcp-Fe/Ir(111). Upper panels show DFT total energies (red squares) and energies obtained via the atomistic spin model (black circles) using DFT parameters for the magnetic interactions (see Supplemental Material for all values). The top axis denotes the noncollinear spin states and the lower axis the corresponding collinear states. Lower panels show the decomposition of the energy into the contributions from the Heisenberg exchange, the biquadratic interaction, the three-site four-spin (3-Spin), and the four-site four-spin interaction (4-Spin). Solid (open) circles represent collinear (noncollinear) states. The lines connecting the data points serve as a guide to the eye. Note that the spin model total energies include the DMI contribution not shown in the decomposition.

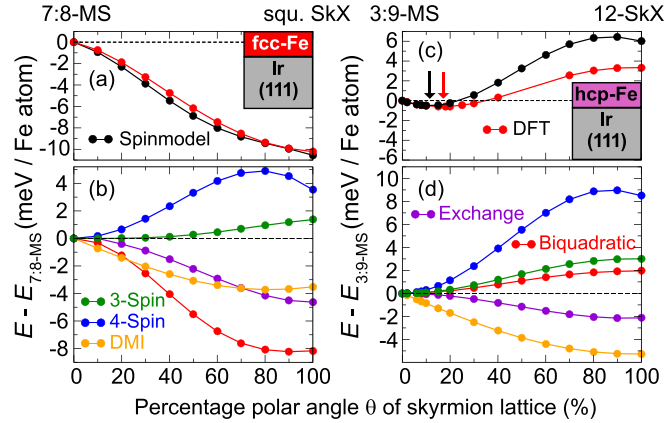

FIG. 4. Total energies of magnetic states along the geodesic path from (a) the square 7:8-MS to the square SkX for fcc-Fe/Ir(111) and (c) the hexagonal 3:9-MS to the hexagonal 12-SkX for hcp-Fe/Ir(111). Red and black data points are obtained via DFT including the effect of SOC and via the atomistic spin model, respectively. (b) and (d) show the energy-resolved contributions from the single magnetic interactions obtained in the atomistic spin model. The relative polar angle θ is defined for every magnetic moment in the unit cell as $\theta(x) = \theta_0 + x(\theta_f - \theta_0)$ with $x \in [0, 1]$ where the value $x = 0$ is chosen for the collinear MS and $x = 1$ for the noncollinear SkX in each case. θ_f refers to the final value of every magnetic moment in the respective SkX, whereas θ_0 is set to 0° for upward pointing moments (180° for downward pointing moments). The lines connecting the data points serve as a guide to the eye.

of magnetic states in which the moments rotate continuously from the 7:8-MS to the square SkX and from the hexagonal 3:9-MS to the 12-SkX, respectively (Fig. 4).

For the square spin lattice of fcc-Fe/Ir(111) [Fig. 4(a)] the fully noncollinear skyrmion lattice clearly represents the energy minimum along the geodesic path in spin space. The atomistic spin model gives an excellent quantitative description of the DFT energies.

In contrast, for the hexagonal 12-atomic state of hcp-Fe/Ir(111) the energy minimum is found to be close to the collinear 3:9-MS in both DFT and spin model [see red/black arrow in Fig. 4(c)]. In the DFT calculation this 18% canted state gains 0.6 meV/Fe atom with respect to the collinear state. Note that the deviation from the collinear MS state corresponds to only 7°–16° of the magnetic moments from the z direction. Hence the degree of noncollinearity is very small. The spin model shows a similar trend of energy versus canting, however, the quantitative deviations are larger than for the square spin lattice [Fig. 4(a)].

The different behavior of square versus hexagonal skyrmion lattices can be explained by the decomposition of the total energy from the spin model [Figs. 4(b) and 4(d)]. In both cases the four-spin interactions favor the collinear MS, while the pairwise exchange and the DMI promote the noncollinear SkX. Due to the opposite sign of the biquadratic term for the two Fe stackings, it favors the noncollinear SkX in fcc-Fe while it stabilizes the collinear MS for hcp-Fe. Quantitatively the contributions of the competing interactions differ between square and hexagonal spin lattices. For the square spin lattice [Fig. 4(b)], the effect of four-spin interactions is weak and the exchange, DMI, and biquadratic term stabilize the SkX. For the hexagonal spin lattice [Fig. 4(d)], the biquadratic and four-spin interactions dominate and a nearly collinear MS occurs [33].

In order to directly compare our prediction of a nearly collinear hexagonal multi-Q state with previous experiments on hcp-Fe/Ir(111) [26], we have simulated SP-STM images (see Supplemental Material [27]). We find that the SP-STM images are very similar for the previously proposed noncollinear 12-SkX and the nearly collinear 3:9-MS state predicted in this Letter irrespective of the magnetization direction of the spin-polarized tip. This makes an unambiguous experimental distinction challenging. However, a similar preference of a hexagonal nearly collinear 12:15-MS over the corresponding SkX has recently been found by DFT for hcp-Fe/Rh/Ir(111) and confirmed by SP-STM experiments [25].

In conclusion, we have demonstrated that the appearance of noncollinear skyrmion lattices versus nearly collinear multi-Q states in Fe monolayers on Ir(111) depends on the symmetry of the spin states due to the interplay of pairwise exchange, higher-order exchange, and DMI. While the magnetic moments in the nanoskyrmion lattice of fcc-Fe/Ir(111)

are strongly canted, we propose that the magnetic ground state of hcp-Fe/Ir(111) is a nearly collinear hexagonal multi-Q state.

We thank André Kubetzka for providing the images of the spin structures shown in Fig. 2 and Gustav Bihlmayer for insightful discussions. We gratefully acknowledge financial support from the Deutsche Forschungsgemeinschaft (DFG, German Research Foundation) via Projects No. 418425860 and No. 462602351 (SPP2137 "Skyrmionics") and computing time provided by the North-German Supercomputing Alliance (HLRN).

[1] S. Mühlbauer, B. Binz, F. Jonietz, C. Pfleiderer, A. Rosch, A. Neubauer, R. Georgii, and P. Boni, Skyrmion lattice in a chiral magnet, Science **323**, 915 (2009).

[2] X. Yu, Y. Onose, N. Kanazawa, J. H. Park, J. Han, Y. Matsui, N. Nagaosa, and Y. Tokura, Real-space observation of a two-dimensional skyrmion crystal, Nature (London) **465**, 901 (2010).

[3] S. Heinze, K. von Bergmann, M. Menzel, J. Brede, A. Kubetzka, R. Wiesendanger, G. Bihlmayer, and S. Blügel, Spontaneous atomic-scale magnetic skyrmion lattice in two dimensions, Nat. Phys. **7**, 713 (2011).

[4] C. Moreau-Luchaire, C. Moutafis, N. Reyren, J. Sampaio, C. A. F. Vaz, N. V. Horne, K. Bouzehouane, K. Garcia, C. Deranlot, P. Warnicke, P. Wohlhüter, J.-M. George, M. Weigand, J. Raabe, V. Cros, and A. Fert, Additive interfacial chiral interaction in multilayers for stabilization of small individual skyrmions at room temperature, Nat. Nanotechnol. **11**, 444 (2016).

[5] O. Boulle, J. Vogel, H. Yang, S. Pizzini, D. de Souza Chaves, A. Locatelli, T. O. Menteş, A. Sala, L. D. Buda-Prejbeanu, O. Klein, M. Belmeguenai, Y. Roussigné, A. Stashkevich, S. M. Chérif, L. Aballe, M. Foerster, M. Chshiev, S. Auffret, I. M. Miron, and G. Gaudin, Room-temperature chiral magnetic skyrmions in ultrathin magnetic nanostructures, Nat. Nanotechnol. **11**, 449 (2016).

[6] S. Woo, K. Litzius, B. Krüger, M.-Y. Im, L. Caretta, K. Richter, M. Mann, A. Krone, R. M. Reeve, M. Weigand, P. Agrawal, I. Lemesh, M.-A. Mawass, P. Fischer, M. Kläui, and G. S. D. Beach, Observation of room-temperature magnetic skyrmions and their current-driven dynamics in ultrathin metallic ferromagnets, Nat. Mater. **15**, 501 (2016).

[7] A. Bogdanov and D. Yablonskii, Thermodynamically stable "vortices" in magnetically ordered crystals. The mixed state of magnets, Sov. Phys. JETP **68**, 101 (1989).

[8] A. Fert, N. Reyren, and V. Cros, Magnetic skyrmions: Advances in physics and potential applications, Nat. Rev. Mater. **2**, 17031 (2017).

[9] C. Back, V. Cros, H. Ebert, K. Everschor-Sitte, A. Fert, M. Garst, T. Ma, S. Mankovsky, T. L. Monchesky, M. Mostovoy, N. Nagaosa, S. S. P. Parkin, C. Pfleiderer, N. Reyren, A. Rosch, Y. Taguchi, Y. Tokura, K. von Bergmann, and J. Zang, The 2020 skyrmionics roadmap, J. Phys. D: Appl. Phys. **53**, 363001 (2020).

[10] I. Dzyaloshinsky, A thermodynamic theory of "weak" ferromagnetism of antiferromagnetics, Sov. Phys. JETP **5**, 1259 (1957).

[11] T. Moriya, New Mechanism of Anisotropic Superexchange Interaction, Phys. Rev. Lett. **4**, 228 (1960).

[12] M. Bode, M. Heide, K. Von Bergmann, P. Ferriani, S. Heinze, G. Bihlmayer, A. Kubetzka, O. Pietzsch, S. Blügel, and R. Wiesendanger, Chiral magnetic order at surfaces driven by inversion asymmetry, Nature (London) **447**, 190 (2007).

[13] T. Okubo, S. Chung, and H. Kawamura, Multiple-q States and the Skyrmion Lattice of the Triangular-Lattice Heisenberg Antiferromagnet under Magnetic Fields, Phys. Rev. Lett. **108**, 017206 (2012).

[14] A. O. Leonov and M. Mostovoy, Multiply periodic states and isolated skyrmions in an anisotropic frustrated magnet, Nat. Commun. **6**, 8275 (2015).

[15] S. von Malottki, B. Dupé, P. Bessarab, A. Delin, and S. Heinze, Enhanced skyrmion stability due to exchange frustration, Sci. Rep. **7**, 12299 (2017).

[16] S. Paul, S. Haldar, S. Malottki, and S. Heinze, Role of higher-order exchange interactions for skyrmion stability, Nat. Commun. **11**, 4756 (2020).

[17] P. Kurz, G. Bihlmayer, K. Hirai, and S. Blügel, Three-Dimensional Spin Structure on a Two-Dimensional Lattice: Mn/Cu(111), Phys. Rev. Lett. **86**, 1106 (2001).

[18] A. Krönlein, M. Schmitt, M. Hoffmann, J. Kemmer, N. Seubert, M. Vogt, J. Küspert, M. Böhme, B. Alonazi, J. Kügel, H. A. Albrithen, M. Bode, G. Bihlmayer, and S. Blügel, Magnetic Ground State Stabilized by Three-Site Interactions: Fe/Rh(111), Phys. Rev. Lett. **120**, 207202 (2018).

[19] N. Romming, H. Pralow, A. Kubetzka, M. Hoffmann, S. von Malottki, S. Meyer, B. Dupé, R. Wiesendanger, K. von Bergmann, and S. Heinze, Competition of Dzyaloshinskii-Moriya and Higher-Order Exchange Interactions in Rh/Fe Atomic Bilayers on Ir(111), Phys. Rev. Lett. **120**, 207201 (2018).

[20] J. Spethmann, S. Meyer, K. von Bergmann, R. Wiesendanger, S. Heinze, and A. Kubetzka, Discovery of Magnetic Single- and Triple-**q** states in Mn/Re(0001), Phys. Rev. Lett. **124**, 227203 (2020).

[21] W. Li, S. Paul, K. von Bergmann, S. Heinze, and R. Wiesendanger, Stacking-Dependent Spin Interactions in Pd/Fe Bilayers on Re(0001), Phys. Rev. Lett. **125**, 227205 (2020).

[22] S. Haldar, S. Meyer, A. Kubetzka, and S. Heinze, Distorted 3Q state driven by topological-chiral magnetic interactions, Phys. Rev. B **104**, L180404 (2021).

[23] M. Gutzeit, S. Haldar, S. Meyer, and S. Heinze, Trends of higher-order exchange interactions in transition metal trilayers, Phys. Rev. B **104**, 024420 (2021).

[24] M. Hoffmann and S. Blügel, Systematic derivation of realistic spin models for beyond-Heisenberg solids, Phys. Rev. B **101**, 024418 (2020).

[25] M. Gutzeit, A. Kubetzka, S. Haldar, H. Pralow, M. Goerzen, R. Wiesendanger, S. Heinze, and K. von Bergmann, Nano-scale collinear multi-Q states driven by higher-order interactions, Nat. Commun. **13**, 5764 (2022).

[26] K. von Bergmann, M. Menzel, A. Kubetzka, and R. Wiesendanger, Influence of the local atom configuration on a hexagonal skyrmion lattice, Nano Lett. **15**, 3280 (2015).

[27] See Supplemental Material at http://link.aps.org/supplemental/10.1103/PhysRevB.108.L060405 for computational details, additional energy dispersions, calculation of higher-order interactions, and SP-STM simulations, which includes Refs. [3,16–18,20,24–26,28,29,34–47].

[28] See https://www.flapw.de

[29] K. von Bergmann, S. Heinze, M. Bode, E. Y. Vedmedenko, G. Bihlmayer, S. Blügel, and R. Wiesendanger, Observation of a Complex Nanoscale Magnetic Structure in a Hexagonal Fe Monolayer, Phys. Rev. Lett. **96**, 167203 (2006).

[30] Note that the 12-SkX state can also occur as an *on-top state* in which the point of constructive interference of the three spin spirals is placed on top of an Fe atom [26]. In contrast, for the 12-SkX state of Fig. 2(c) this point is on a hollow site. Within our DFT calculations, the *on-top* and *hollow* 12-SkX states are energetically nearly degenerate (see Supplemental Material [27]).

[31] Note that the energies of all spin spiral ($1Q$) states in the spin model are equal to the DFT values.

[32] Note that going beyond the model of nearest-neighbor higher-order interaction (HOI) might change the values of the constants. However, the main point here is that a model of only nearest-neighbor HOI can explain the stabilization of a non-collinear square skyrmion lattice versus a collinear hexagonal multi-Q state and can reproduce the trend of the DFT total energies (Fig. 3, top panels). We have excluded anisotropic higher-order interactions in the spin model since including SOC does not alter the trend of the DFT total energies seen in Fig. 3.

[33] Note that K_1 is of similar magnitude for both Fe stackings while B_1 and Y_1 are much smaller for hcp-Fe (cf. Table I).

[34] P. Kurz, F. Förster, L. Nordström, G. Bihlmayer, and S. Blügel, *Ab initio* treatment of noncollinear magnets with the full-potential linearized augmented plane wave method, Phys. Rev. B **69**, 024415 (2004).

[35] M. Heide, G. Bihlmayer, and S. Blügel, Describing Dzyaloshinskii-Moriya spirals from first principles, Phys. B: Condens. Matter **404**, 2678 (2009).

[36] P. E. Blöchl, Projector augmented-wave method, Phys. Rev. B **50**, 17953 (1994).

[37] See https://www.vasp.at/.

[38] G. Kresse and J. Furthmüller, Efficient iterative schemes for *ab initio* total-energy calculations using a plane-wave basis set, Phys. Rev. B **54**, 11169 (1996).

[39] G. Kresse and D. Joubert, From ultrasoft pseudopotentials to the projector augmented-wave method, Phys. Rev. B **59**, 1758 (1999).

[40] B. Dupé, M. Hoffmann, C. Paillard, and S. Heinze, Tailoring magnetic skyrmions in ultra-thin transition metal films, Nat. Commun. **5**, 4030 (2014).

[41] J. P. Perdew, J. A. Chevary, S. H. Vosko, K. A. Jackson, M. R. Pederson, D. J. Singh, and C. Fiolhais, Atoms, molecules, solids, and surfaces: Applications of the generalized gradient approximation for exchange and correlation, Phys. Rev. B **46**, 6671 (1992).

[42] J. P. Perdew, K. Burke, and M. Ernzerhof, Generalized Gradient Approximation Made Simple, Phys. Rev. Lett. **77**, 3865 (1996).

[43] K. von Bergmann, S. Heinze, M. Bode, G. Bihlmayer, S. Blügel, and R. Wiesendanger, Complex magnetism of the Fe monolayer on Ir(111), New J. Phys. **9**, 396 (2007).

[44] C. Li, A. J. Freeman, H. J. F. Jansen, and C. L. Fu, Magnetic anisotropy in low-dimensional ferromagnetic systems: Fe monolayers on Ag(001), Au(001), and Pd(001) substrates, Phys. Rev. B **42**, 5433 (1990).

[45] S. H. Vosko, L. Wilk, and M. Nusair, Accurate spin-dependent electron liquid correlation energies for local spin density calculations: a critical analysis, Can. J. Phys. **58**, 1200 (1980).

[46] S. Heinze, Simulation of spin-polarized scanning tunneling microscopy images of nanoscale non-collinear magnetic structures, Appl. Phys. A **85**, 407 (2006).

[47] B. Hardrat, A. Al-Zubi, P. Ferriani, S. Blügel, G. Bihlmayer, and S. Heinze, Complex magnetism of iron monolayers on hexagonal transition metal surfaces from first principles, Phys. Rev. B **79**, 094411 (2009).